IEEE Photonics Journal
An IEEE Photonics Society Publication

Open Access

Visible Light Channel Modeling for Gas Pipelines

Volume 10, Number 2, April 2018

Farshad Miramirkhani, *Student Member, IEEE*
Murat Uysal, *Senior Member, IEEE*
Omer Narmanlioglu, *Student Member, IEEE*
Mohamed Abdallah, *Senior Member, IEEE*
Khalid Qaraqe, *Senior Member, IEEE*

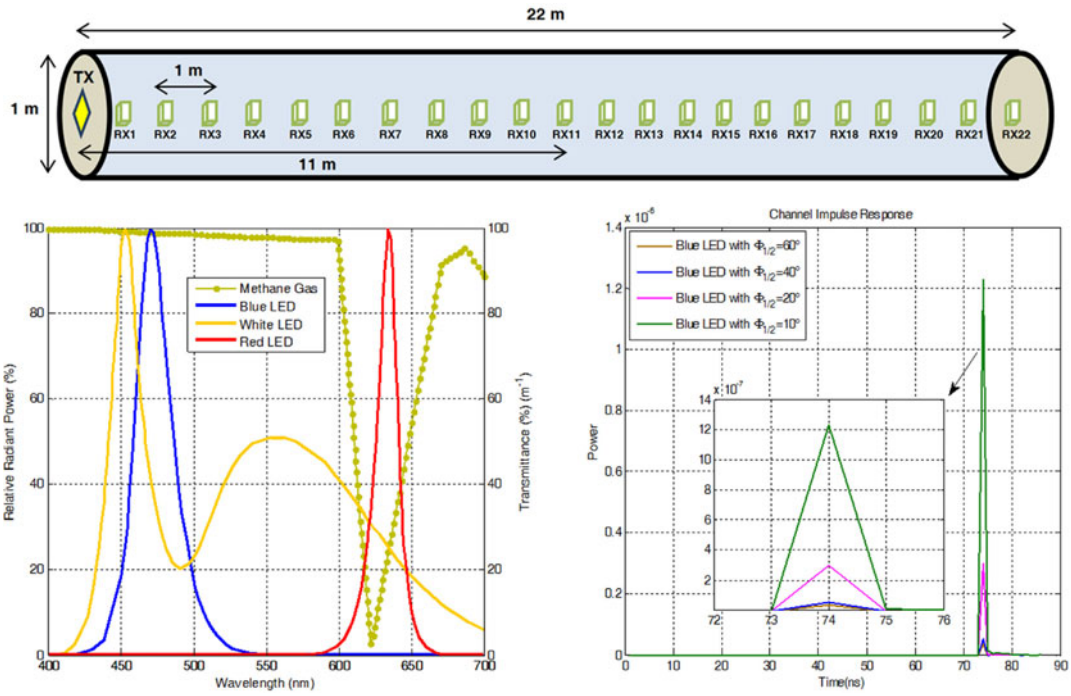

DOI: 10.1109/JPHOT.2018.2819723
1943-0655 © 2018 IEEE

IEEE photonics SOCIETY

IEEE

Visible Light Channel Modeling for Gas Pipelines

Farshad Miramirkhani,[1] ***Student Member, IEEE***,
Murat Uysal,[1] ***Senior Member, IEEE***,
Omer Narmanlioglu,[1] ***Student Member, IEEE***,
Mohamed Abdallah,[2] ***Senior Member, IEEE***,
and Khalid Qaraqe,[3] ***Senior Member, IEEE***

[1]Department of Electrical and Electronics Engineering, Ozyegin University, Istanbul 34794, Turkey
[2]College of Science and Engineering, Hamad Bin Khalifa University, Doha 34110, Qatar
[3]Department of Electrical and Computer Engineering, Texas A&M University at Qatar, Doha 23874, Qatar

DOI:10.1109/JPHOT.2018.2819723

Manuscript received September 15, 2017; revised March 20, 2018; accepted March 22, 2018. Date of publication March 26, 2018; date of current version April 17, 2018. This work was supported by the NPRP award under Grant NPRP 8-648-2-273 from the Qatar National Research Fund (a member of the Qatar Foundation). Corresponding author: Farshad Miramirkhani (e-mail: fmiramirkhani@yahoo.com).

Abstract: In this paper, we explore the use of visible light communication as a means of wireless monitoring in gas pipelines. In an effort to shed light on the communication limits in the presence of gas, we create a three-dimensional simulation platform where the pipeline size/shape, the reflection characteristics of the interior coating, gas specifications (i.e., temperature, density, refractive index, transmittance, etc.) and the specifications of the light sources and detectors (i.e., field of view, lighting pattern, etc.) are precisely defined. Based on ray tracing, we obtain channel impulse responses within the gas pipeline considering the deployment of different colored LEDs with various viewing angles. We further investigate the maximum achievable link range to ensure a given bit error rate.

Index Terms: Visible light communications, channel modeling, ray tracing, downhole monitoring.

1. Introduction

In oil and gas industry, the ability to communicate between downhole and surface instruments has become a critical need as operators promote production efficiency and the optimization of well performance. The use of wirelines and armored cables [1]–[7] for this purpose is common in the industry, but these installations present maintenance and reliability issues. Furthermore, wireline solutions come with high installation costs and their operation requires the halt of production bringing extra cost to the operator due to off-time. Various forms of wireless monitoring such as mud-pulse telemetry [8]–[10], low-frequency electromagnetic waves (e.g., 2–12 Hz) [11]–[13] and acoustic signaling [14]–[16] have been reported in the literature.

The restrictions of existing technologies require a new and reliable wireless solution for real-time downhole monitoring. In this paper, we propose a wireless telemetry solution based on visible light communication (VLC) [17]. So far, the only work which has investigated VLC for downhole monitoring is reported in [18]. However, the channel model in [18] builds upon ideal Lambertian

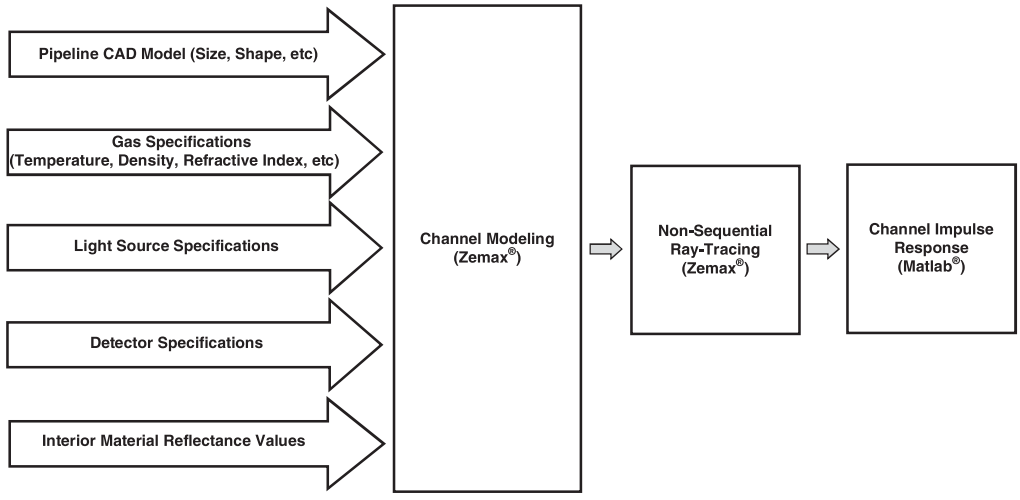

Fig. 1. Overview of major steps in channel modeling approach.

source and considers only purely diffuse reflections. Furthermore, it assumes an empty pipeline and does not consider the effect of gas.

In this paper, we investigate the propagation characteristics of the downhole VLC channel based on ray tracing [19]. The simulation environment is created in Zemax® where the CAD model of the pipeline and light sources (i.e., LEDs) are integrated. Reflection characteristics of the interior coating and gas specifications are further provided as inputs. Non-sequential ray tracing is then used to determine the detected power and path lengths from source to detector for each ray. These are then used to construct the channel impulse response (CIR). In our work, we explore the use of white, blue and red LEDs with different field of views. Based on CIRs, we also investigate the maximum achievable distance in the pipeline to ensure a given bit error rate.

The remainder of the paper is organized as follows. In Section 2, we describe the methodology adopted for channel modeling. In Section 3, we present CIRs for a pipeline with and without gas and investigate the effect of LED specifications (i.e., viewing angle and wavelength) on the channel parameters such as channel DC gain and root mean square (RMS) delay spread. In Section 4, we investigate the achievable link range and propose a multi-hop transmission scheme to increase the link range. We finally conclude in Section 5.

2. Channel Modeling Approach and Simulation Setup

Overview of our channel modelling approach, based on ray tracing features of ZemaxR, can be found in [19]. A summary of major steps is illustrated in Fig. 1. In the first step, a three dimensional simulation platform for pipeline is created in ZemaxR where its size, shape, the reflection characteristics of the interior coating, gas specifications (i.e., temperature, density, refractive index, transmission, etc) and the specifications of the light sources and detectors (i.e., field of view, lighting pattern, etc) are precisely defined.

The pipeline under consideration is used for transport of Liquefied Natural Gas (LNG) and has a cylindrical shape with a length of 22 meters and a diameter of 1 meter (see Fig. 2). The interior of pipeline is carbon steel [20]. As a wireless transmitter, an LED (i.e., denoted as TX) is located at the head of the pipeline. Receiver test points with 1 meter apart from each other are assumed within the pipeline. These are denoted as RX1, RX2,. . . , RX22. Each detector is assumed to have an area of 1 cm^2 and a field of view (FOV) of 85°.

Natural gas is composed primarily of methane, but may also contain ethane, propane and heavier hydrocarbons. Small quantities of nitrogen, oxygen, carbon dioxide, sulfur compounds, and water

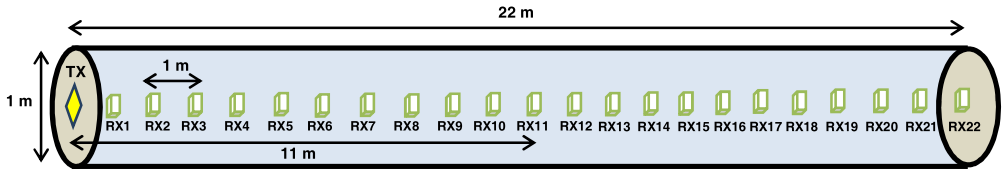

Fig. 2. Illustration of gas pipeline under consideration.

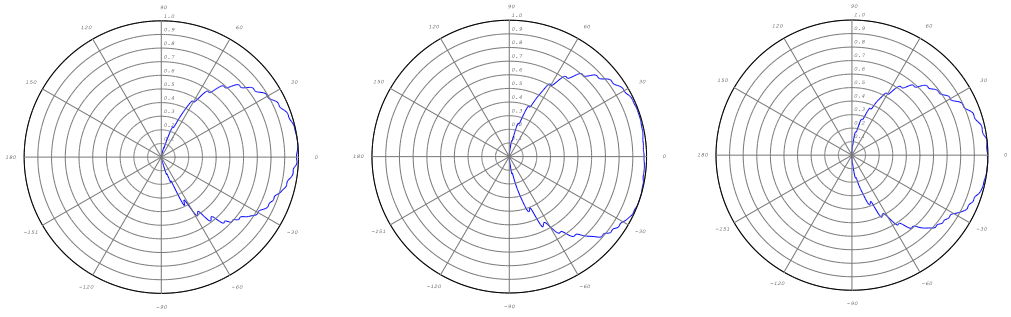

Fig. 3. Emission pattern of source for (a) white Cree Xlamp® MC-E (b) blue Cree Xlamp® XP-C (c) red Cree Xlamp® XP-C.

may also be found in natural gas. The liquefaction process requires the removal of some of the non-methane components such as water and carbon dioxide from the produced natural gas to prevent them from forming solids when the gas is cooled to about LNG temperature. Methane is by far the major component over 95% by volume for LNG [21]. Therefore, in our study, we assume the presence of only methane gas in the pipeline. Density, wavelength-dependent refractive index and transmission values of methane gas at 111K can be found in [22] and [23].

As transmitters, we consider white, blue and red LEDs commercially available from Cree®. A widely adopted approach to generate white light is to excite yellow phosphor coating with a blue LED. It is however known that the slow response of the phosphor limits the modulation bandwidth in the white LED. For example, a bandwidth of ∼2.5 MHz is reported in [24] for white LEDs. On the other hand, blue and red LEDs have larger modulation bandwidths [25] and [26] exceeding 10 MHz. unless otherwise stated, the half viewing angle of LEDs is 60° (see Fig. 3 for the LED emission patterns). Fig. 4 illustrates the relative radiant power of the LEDs under consideration as well as the transmittance of methane gas in the visible range, respectively. It is observed from Fig. 4 that the maximum transmittance of methane is in the range of 464 nm–478 nm (i.e., blue color) while the minimum transmittance is in the range of 617 nm–631 nm (i.e., red color). This indicates that blue colored LEDs should be deployed to minimize path loss as much as possible.

Non-sequential ray tracing features of ZemaxR are used to calculate the detected optical power and path lengths from source to detector for each ray. In ray tracing, the source emits the rays based on a given statistical distribution (distribution type depends on the source). Rays are then traced along a physically realizable path until they intercept an object. Through “Table Glass Method” [27] in ZemaxR, we also define the density, wavelength-dependent refractive index and transmission value of gas in the pipeline. This allows the characterization of interaction of rays with the medium. In addition to the line-of-sight (LOS) components, there might be a number of reflections from pipeline boundaries. ZemaxR non-sequential ray-tracing tool generates an output file which includes the detected power and path lengths for each ray. This data is imported to MATLAB® and using these information, the CIR is expressed as [19]

$$h(t) = \sum_{i=1}^{N_r} P_i \delta(t - \tau_i) \tag{1}$$

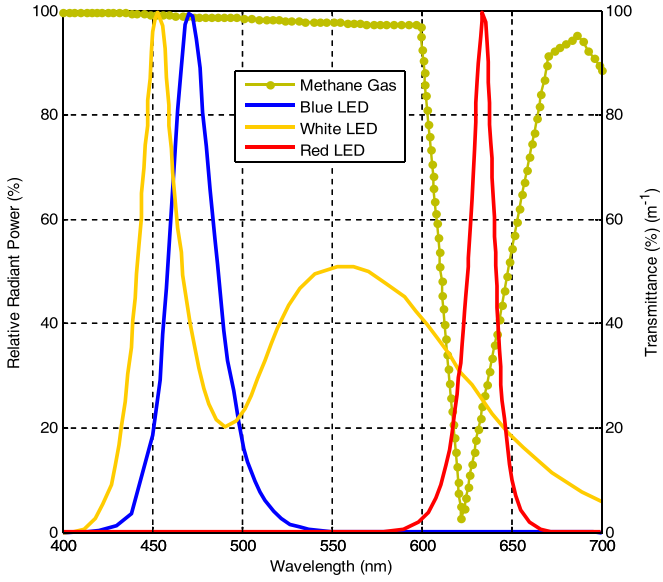

Fig. 4. Relative radiant power of white, blue and red LEDs and the transmittance of methane gas in the visible range.

where P_i is the power of the ith ray, τ_i is the propagation time of the ith ray, $\delta(t)$ is the Dirac delta function and N_r is the number of rays received at the detector. The frequency response of the optical channel can be further obtained through the Fourier transform, i.e.,

$$H(f) = F[h(t)] = \int \sum_{i=1}^{N_r} P_i \, \delta(t - \tau_i) \, e^{-j2\pi ft} dt \tag{2}$$

To quantify channel characteristics, path loss, DC gain and RMS delay spread are commonly used. Based on the obtained CIR in (1), the path loss is expressed as [28]

$$PL = -10 \log_{10} \left(\int_0^\infty h(t) \, dt \right) \tag{3}$$

Channel DC gain and RMS delay spread are respectively defined as [19]

$$H_0 = H(0) = \int_0^\infty h(t) \, dt \tag{4}$$

$$\tau_{RMS} = \sqrt{\frac{\int_0^\infty (t - \tau_0)^2 h(t) \, dt}{\int_0^\infty h(t) \, dt}} \tag{5}$$

where τ_0 is the mean excess delay spread.

3. Pipeline Channel Impulse Responses

Based on the methodology summarized in Section 2, we run simulations and obtain the CIRs for all 22 receiver test points within the pipeline. As examples, we provide sample CIRs in Fig. 5 where the receiver is located at the head, middle and end of the pipeline, i.e., RX1, RX11 and RX22. These are denoted as $h_1(t)$, $h_{11}(t)$ and $h_{22}(t)$, respectively. The CIRs obtained for empty pipeline at the same locations are further included as benchmarks.

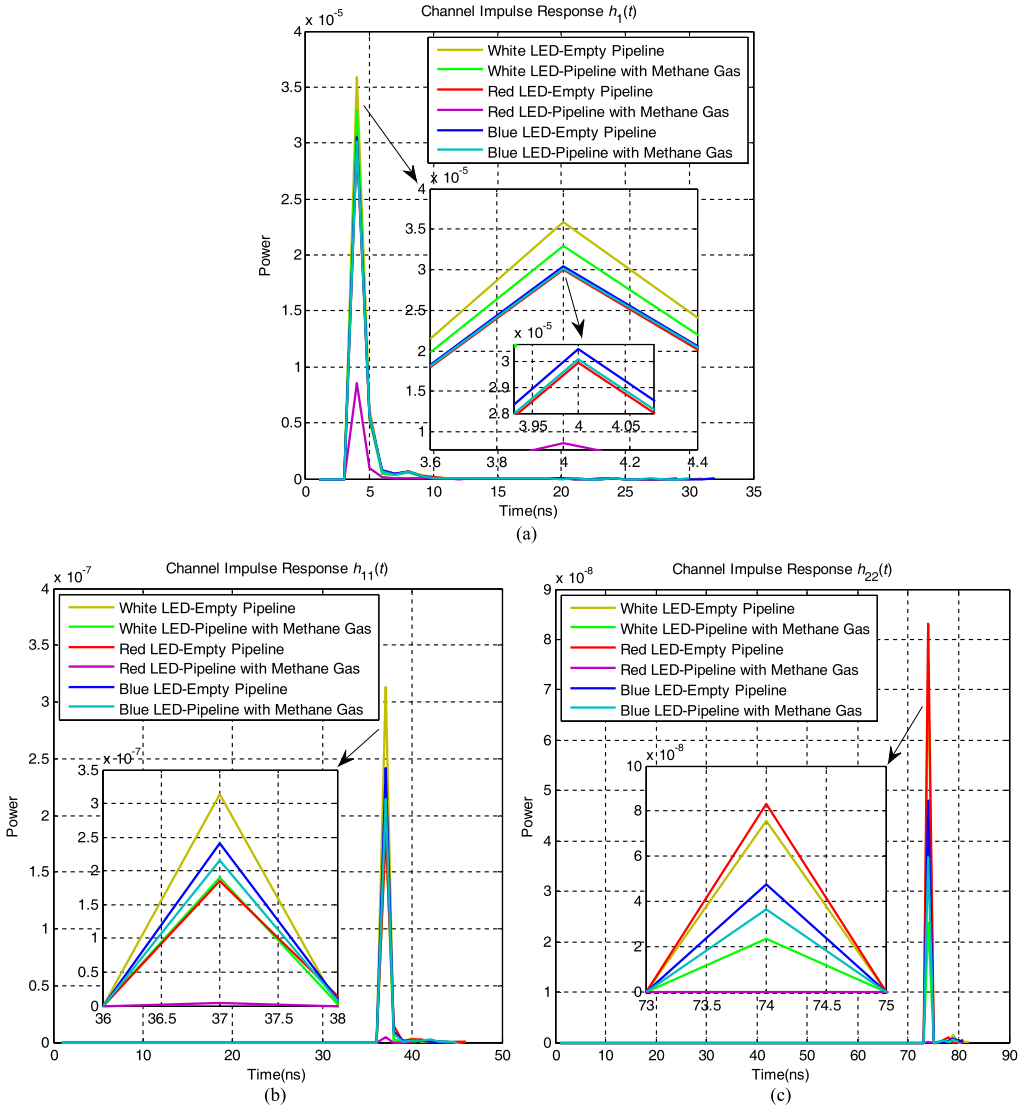

Fig. 5. CIRs for (a) RX1 (b) RX11 and (c) RX22.

The path losses for empty pipeline and pipeline with methane gas respectively are listed in Tables 1 and 2. It is observed from these tables that the path losses obtained with red LED are larger than those ones obtained with blue and white LEDs. This is as a result of the fact that the minimum transmittance of methane gas is in the red band (i.e., 617 nm–631 nm). It is also revealed from Tables 1 and 2 that the path losses obtained with white LED are more or less same as those obtained with the blue LED. Since the illumination purposes are not of concern in telemetry application under consideration, we choose blue LED with larger bandwidth as the transmitter in the rest of this study.

In Fig. 6, we investigate the effect of half viewing angle of LED on the CIR. We assume a pipeline with methane gas, use blue LED and vary half viewing angle in the range of 10°–60°. It is observed that as half viewing angle decreases, the number of reflected rays decreases and LOS channel gain increases. Particularly, channel DC gain is equal to 3.80×10^{-8} for 60° while it increases to 1.26×10^{-6} for 10°.

TABLE 1
Path Losses for Empty Pipeline (in dB)

LED	RX1	RX11	RX22
White	43.55	64.96	71.09
Red	44.22	66.86	70.70
Blue	44.15	65.90	73.03

TABLE 2
Path Losses for Pipeline With Methane Gas (in dB)

LED	RX1	RX11	RX22
White	43.99	67.12	76.17
Red	50.13	83.90	106.81
Blue	44.20	66.42	74.20

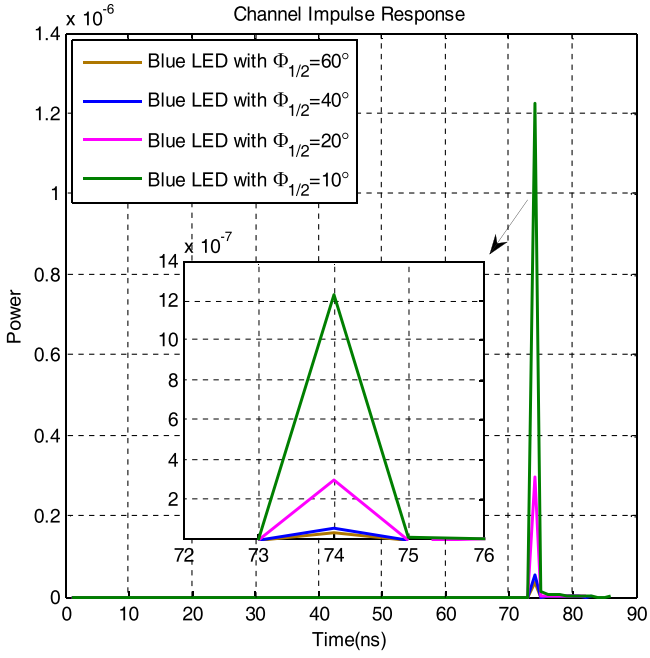

Fig. 6. CIR of pipeline with methane gas for blue LED with different half viewing angles.

4. Achievable Link Ranges

In addition to the multipath propagation environment, the effect of LED response should be further taken into account in the channel modeling [29]. To reflect the low pass nature of LED, its frequency response is typically modelled as [30]

$$H_{\text{LED}}(f) = \frac{1}{1 + jf/f_{\text{cut-off}}} \tag{6}$$

where $f_{\text{cut-off}}$ is the LED 3-dB cut-off frequency. The *effective* channel frequency response (taking into account the LED characteristics) can be then expressed as

$$H_{\text{eff}}(f) = H_{\text{LED}}(f)\, H(f) \tag{7}$$

Fig. 7 illustrates the frequency response of pipeline with methane gas for blue LED with different half viewing angles. In this figure, we assume $f_{\text{cut-off}} = 14\,\text{MHz}$ [25]. Let B_s denote the data rate.

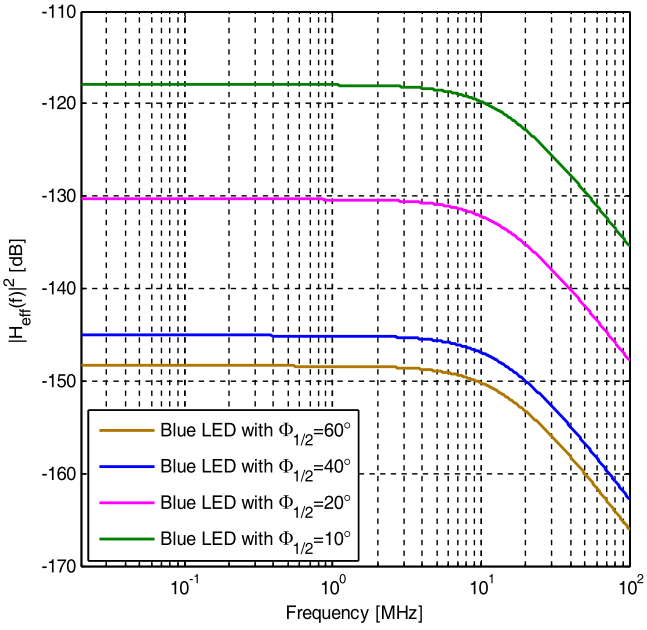

Fig. 7. Effective frequency response of pipeline with methane gas for blue LED with different half viewing angles.

A channel is classified as frequency-selective for $B_s\tau_{RMS} \geq 1$. If $B_s\tau_{RMS} \ll 1$, then it is classified as frequency-flat channel. Based on the CIR in Fig. 6 (i.e., blue LED with $\Phi_{1/2} = 10^{\circ}$), the RMS delay spread for a pipeline with methane gas is calculated as 11.37 ns at RX22. This indicates that for signaling rates lower than 8.79 Msample/sec which can be easily justified for practical needs in pipeline monitoring, the multipath components are not resolvable and the channel can be modeled as a single-tap (frequency-flat) channel.

We assume the use of M-ary pulse amplitude modulation (PAM) where M is constellation size. Under the assumption of frequency-flat channel response, bit error rate (BER) for high SNR region is given by [31]

$$BER \approx \frac{2\,(M-1)}{M \log_2 (M)} Q\left(\frac{1}{M-1}\sqrt{\frac{(r h_{\text{eff}} P_t)^2 T_s}{N_0}}\right) \tag{8}$$

where $h_{\text{eff}} = \int_0^{\infty} h_{\text{eff}}(t)\,dt$, and $h_{\text{eff}}(t) = F^{-1}[H_{\text{eff}}(f)] = \int H_{\text{eff}}(f) e^{j2\pi ft} df$. In (8), r is the responsivity of photodetector, P_t is the average transmitted optical power, N_0 is the noise power spectral density and T_s is the sampling interval. Based on (8), the minimum gain of the channel that satisfies a given BER target can be obtained by

$$h_{\text{eff}}^2 \approx \frac{N_0}{(r P_t)^2 T_s}\left((M-1)\,Q^{-1}\left(\frac{M \log_2 (M)\, BER}{2\,(M-1)}\right)\right)^2 \tag{9}$$

Assume that targeted BER is 10^{-6}. Furthermore, set $r = 0.28$ A/W [32], $P_t = 50$ mWatt, $N_0 = 10^{-22}$ W/Hz and $T_s = 1$ msec. Based on the earlier obtained CIRs, we obtain the maximum distance where target BER is satisfied for different sizes of PAM (see Table 3). It can be noted that the whole pipeline can be covered with the use of 2-PAM, 4-PAM and 8-PAM since they satisfy the given BER target at 22 m. On the other hand, the maximum distance that can be covered by 16-PAM is 19.07 m. After this point, BER becomes higher than 10^{-6}. Similarly, the maximum distances that can be covered by 32-PAM, 64-PAM, 128-PAM, 256-PAM and 512-PAM, respectively are 13.64 m, 9.99 m, 7.32 m, 5.28 m and 3.82 m.

TABLE 3
Maximum Distance Values Where Target BER is Satisfied With Given Modulation Order

Modulation	Maximum Distance (m)
2-PAM	> 22
4-PAM	> 22
8-PAM	> 22
16-PAM	19.07
32-PAM	13.64
64-PAM	9.99
128-PAM	7.32
256-PAM	5.28
512-PAM	3.82

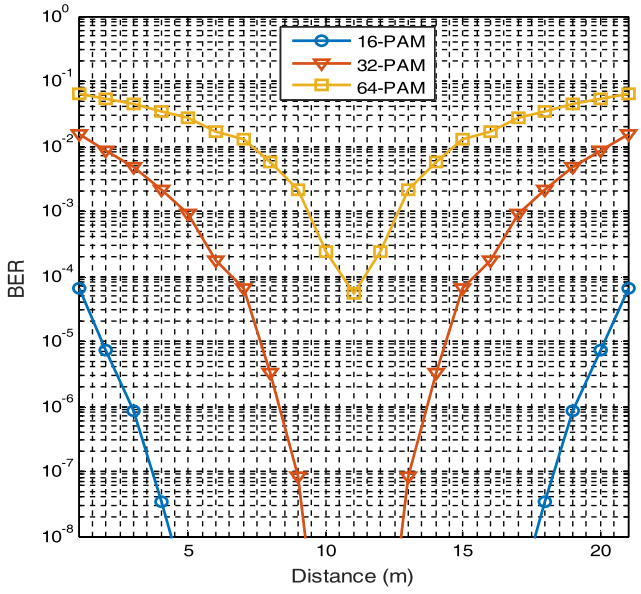

Fig. 8. BER performance of multi-hop transmission including one relay terminal located at different distances.

As modulation size is increased, the maximum distance for reliable transmission decreases. For such cases (i.e., $M \geq 16$), multi-hop transmission can be used to enable connectivity within the pipeline. In the following, we consider detect-and-forward relaying. Deployment of single relay is assumed. The relay terminal first detects the received signal from source terminal (S), re-modulates, and then forwards it to the destination (D). In Fig. 8, we illustrate the BER performance assuming that the relay terminal is located at different distances with respect to source. It is observed that for 16-PAM when the relay is located between 2.90 m and 19.10 m, the targeted BER is satisfied. Similarly, for 32-PAM, it is satisfied when the relay is located between 8.30 m and 13.70 m. On the other hand, for higher order PAM, i.e., 64-PAM, 128-PAM and 512-PAM, more than one relay terminal is required in order to satisfy BER target at 22 m.

5. Conclusion

In this paper, we explored the potential use of VLC technology in gas pipelines. Taking advantage of the advanced ray tracing features of ZemaxR, we obtained realistic CIRs inside the gas pipeline.

Our results demonstrated that path loss effects are less pronounced for white and blue LEDs in a pipeline filled with methane gas. Since blue LEDs have typically larger bandwidths, they become the natural choice for this application where illumination is not of concern. We further investigated the achievable link range to ensure a given BER assuming the use of PAM. As modulation size is increased, the maximum distance for reliable transmission decreases. For a BER target of 10^{-6}, PAM modulation size up to $M = 8$ can be used to cover the pipeline with a length of 22 m under consideration. For 16-PAM, the maximum achievable distance reduces to 19.07 m. That indicates that a single hop will not be sufficient to cover the pipeline. Achievable distances for 32-PAM, 64-PAM, 128-PAM, 256-PAM and 512-PAM further reduce to 13.64 m, 9.99 m, 7.32 m, 5.28 m and 3.82 m, respectively. For such cases, we proposed multi-hop transmission to enable connectivity within the pipeline. While a single relay is sufficient for 16-PAM and 32-PAM, PAM with higher order modulation sizes requires more than one relay terminal to satisfy the BER target of 10^{-6}.

Acknowledgment

The statements made herein are solely the responsibility of the authors.

References

[1] T. H. Ali *et al.*, "High speed telemetry drill pipe network optimizes drilling dynamics and wellbore placement," in *Proc. IADC Drilling Conf., Soc. Petroleum Eng.*, Jan. 2008.
[2] D. V. Ellis and J. M. Singer, *Well Logging for Earth Scientists*, 2nd ed. Berlin, Germany: Springer-Verlag, 2007.
[3] K. Bybee, "High-speed wired-drillstring telemetry," *J. Petroleum Technol.*, vol. 60, no. 12, pp. 76–78, 2008.
[4] M. Hernandez *et al.*, "The first offshore use of an ultrahigh-speed drillstring telemetry network involving full LWD logging suite and rotary-steerable drilling system," in *Proc. Annu. Tech. Conf. Exhib., Soc. Petroleum Eng.*, Nov. 2007.
[5] M. J. Jellison *et al.*, "Telemetry drill pipe: Enabling technology for the downhole internet," in *Proc. IADC Drilling Conf., Soc. Petroleum Eng.*, Jan. 2003.
[6] M. J. Jellison *et al.*, "Intelligent drill pipe creates the drilling network," in *Proc. Asia Pac. Oil Gas Conf., Soc. Petroleum Eng.*, Jan. 2003.
[7] M. J. Manning *et al.*, "Processing wired pipe LWD-FE data in real time-experiences and lessons learned," in *Proc.48th Annu. Logging Symp., Soc. Petrophys. Well-Log Anal.*, Jun. 2007.
[8] W. Emmerich, O. Akimov, I. B. Brahim, and E. A. Greten, "Reliable high-speed mud pulse telemetry," in *Proc. IADC Drilling Conf., Soc. Petroleum Eng.*, Mar. 2015.
[9] C. Klotz, P. Bond, and I. Wasserman, "A new mud-pulse telemetry system for enhanced MWD/LWD applications," in *Proc. IADC Drilling Conf., Soc.Petroleum Eng.*, Mar. 2008.
[10] J. R. Jorden and F. L. Campbell, *Well Logging II: Electric and Acoustic Logging*, 1st ed. Richardson, TX, USA: Society of Petroleum Engineers, 1986.
[11] Y. Su *et al.*, "Electromagnetic measurement while drilling technology based on the carrier communication principle," *Petroleum Exp. Dev.*, vol. 40, no. 2, pp. 242–248, 2013.
[12] X. Hao and H. Binjie, "Electromagnetic transmission channel study of MWD," *Chin. J. Geophys.*, vol. 40, no. 3, 1997.
[13] J. Schnitger and J. Macpherson, "Signal attenuation for electromagnetic telemetry systems," in *Proc. SPE/IADC Drilling Conf. Exhib., Soc .Petroleum Eng.*, 2009.
[14] M. Azari *et al.*, "Real time data acquisition with advanced acoustic telemetry improves operational efficiency in deep water offshore well testing," in *Proc. SPE Asia Pac. Oil Gas Conf. Exhib., Soc. Petroleum Eng.*, Jan. 2006.
[15] M. E. Reeves, P. L. Camwell, and J. McRory, "High speed acoustic telemetry network enables real-time along string measurements, greatly reducing drilling risk," in *Proc. offshore Eur., Soc. Petroleum Eng.*, Jan. 2011, pp. 458–469.
[16] L. Gao *et al.*, "Acoustic telemetry can deliver more real-time downhole data in underbalanced drilling operations," in *Proc. IADC/SPE Drilling Conf., Soc. Petroleum Eng.*, 2006.
[17] M. Uysal, C. Capsoni, Z. Ghassemlooy, A. Boucouvalas, and E. Udvary, *Optical Wireless Communications: An Emerging Technology*. Berlin, Germany: Springer, 2016.
[18] Y. Li, S. Videv, M. Abdallah, K. Qaraqe, M. Uysal, and H. Haas, "Single photon avalanche diode (SPAD) VLC system and application to downhole monitoring," in *Proc. IEEE Global Commun. Conf.*, Austin, TX, USA, 2014, pp. 2108–2113.
[19] F. Miramirkhani and M. Uysal, "Channel modeling and characterization for visible light communications," *IEEE Photon. J.*, vol. 7, no. 6, Dec. 2015.
[20] Q. Li *et al.*, "Synergistic effects of passivation treatment and nano-electrodeposition technologies on corrosion protection performance of the electrogalvanized steel," *New J. Chem.*, vol. 39, no. 12, pp. 9903–9909, 2015.
[21] B. G. Liptak and K. Venczel, *Analysis and Analyzers*, vol. II, 5th ed. Boca Raton, FL, USA: CRC Press, 2016.
[22] 2018. [Online]. Available: http://refractiveindex.info/?shelf=organic&book=methane&page=Martonchik-liquid-111K
[23] J. V. Martonchik and G. S. Orton, "Optical constants of liquid and solid methane," *Appl. Opt.*, vol. 33, no. 36, pp. 8306–8317, 1994.
[24] D. C. O'Brien *et al.*, "High-speed visible light communications using multiple-resonant equalization," *IEEE Photon. Tech. Lett.*, vol. 20, no. 14, pp. 1243–1245, Jul. 2008.

[25] L. Zeng *et al.*, "High data rate multiple input multiple output (MIMO) optical wireless communications using white LED lighting," *IEEE J. Sel. Areas Commun.*, vol. 27, no. 9, pp. 1654–1662, Dec. 2009.
[26] B. Fahs *et al.*, "A 6-m OOK VLC link using CMOS-compatible p-n photodiode and red LED," *IEEE Photon. Tech. Lett.*, vol. 28, no. 24, pp. 2846–2849, Dec. 2016.
[27] Zemax 13 Release 2, Radiant Zemax LLC, 2005. [Online]. Available: http://www.zemax.com/os/resources/learn/knowledgebase/how-to-enter-glass-data-at-specific-wavelengths
[28] F. Miramirkhani, O. Narmanlioglu, M. Uysal, and E. Panayirci, "A mobile channel model for VLC and application to adaptive system design," *IEEE Commun. Lett.*, vol. 21, no. 5, pp. 1035–1038, May 2017.
[29] M. Uysal, F. Miramirkhani, O. Narmanlioglu, T. Baykas, and E. Panayirci, "IEEE 802.15.7r1 reference channel models for visible light communications," *IEEE Commun. Mag.*, vol. 55, no. 1, pp. 212–217, Jan. 2017.
[30] L. Grobe and K. D. Langer, "Block-based PAM with frequency domain equalization in visible light communications," in *Proc. IEEE Globecom Workshops*, 2013, pp. 1070–1075.
[31] T. Fath and H. Haas, "Performance comparison of MIMO techniques for optical wireless communications in indoor environment," *IEEE Trans. Commun.*, vol. 61, no. 2, pp. 733–742, Feb. 2013.
[32] J. Grubor, S. Randel, K. D. Langer, and J. W. Walewski, "Broadband information broadcasting using LED-based interior lighting," *J. Lightw. Technol.*, vol. 26, no. 24, pp. 3883–3892, Dec. 2008.